ACS NANO
Cite This: ACS Nano 2019, 13, 14348−14356
www.acsnano.org

ARTICLE

Highly Precise Multifunctional Thermal Management-Based Flexible Sensing Sheets

Kaichen Xu,[†] Yuyao Lu,[†] Takafumi Yamaguchi,[†] Takayuki Arie,[†] Seiji Akita,[†] and Kuniharu Takei*[,†,‡]

[†]Department of Physics and Electronics, Osaka Prefecture UniversitySakai, Osaka 599-8531, Japan
[‡]JST PRESTO, Kawaguchi, Saitama 332-0012, Japan

Supporting Information

ABSTRACT: **Elaborate manipulation of heat transfer renders proper operation of diverse thermal-related technologies. However, accurate implementation of thermal-based or transduction sensing on a thin flexible film over unusual surfaces remains challenging. Herein, efficient thermal management realizes highly accurate flexible multifunctional sensor sheets using a low thermal conductive medium as a thermal barrier. An approximately 50-fold enhancement in the thermal sensing accuracy, which is nearly independent of the changes in the external surroundings, is achieved. Such rational control of heat convection and conduction allows to not only dynamically monitor air flow, but also sight the large-scale air flow distribution on curved surfaces using a flexible thermal flow sensor array. Additionally, accurate wearable skin temperature monitoring independent of the sudden surrounding variations is achieved. This work addresses the formidable challenge of untethered heat transfer induced imprecise thermal related sensing, which universally exists in skin-inspired Internet of Things (IoT) applications.**

KEYWORDS: *thermal management, flexible sensors, wearable electronics, thermal flow sensor array, internet of things*

Judicious regulation of thermal energy transfer propels the development of ubiquitous modern technologies such as integrated electronic devices,[1] light-emitting elements,[2] aircraft and aerospace units,[3] energy generation and storage systems,[4] and elaborate textiles.[5] In principle, heat transfer involves thermal conduction, convection, and radiation. These processes account for the majority of thermal energy-related techniques. For instance, one strategy to maintain body temperature through dexterously regulating heating and cooling is radiative thermoregulatory textiles. Such textiles diminish building-level energy consumption while simultaneously improving human-body comfort.[5−7] Furthermore, the rapid miniaturization of electronic systems with ever growing power densities poses challenges as thermally conductive yet insulating materials must continually be developed to effectively dissipate heat in the case of performance degradation.[8−10]

Another promising subfield based on thermal management is skin-inspired thermal sensing. This is typically used to monitor the targeted temperature itself[11] or transduction of the thermal signals into other valuable physical and biological information such as pressure/strain,[12,13] wind flow,[14] respiration,[15] or blood[16] through heat transfer. Among these flexible thermal-based sensing systems, temperature sensors are generally incorporated for detection of temperature fluctuations or thermal compensation.[11,17] However, accurate thermal related sensing based on a thin flexible film is challenging due to the untethered heat transfer between an objective surface and its surroundings. Consequently, thermal perception is generally limited to a localized governable space.

To realize precise thermal associated sensing over a variety of surfaces, this study proposes a multifunctional flexible thermal management-based sensing sheet by incorporating a low thermal conductive medium. The fundamental properties of thermal barriers are investigated under extreme ambient changes. By rationally arranging the sensor configuration based on a calorimetric sensing mechanism, the macroscale flexible device enables to dynamically monitor the air flow distribution without disturbing the pristine nature of flow. Flexible macroscale sheet-based air flow mapping is implemented on high thermal conductive stages and curved surfaces by deliberately manipulating thermal conduction and convection. Furthermore, accurately monitoring temperature fluctuations on skin is realized on the basis of such efficient thermal management even if the temperature of the surrounding changes abruptly. This work affords a pathway to conceive

Received: October 2, 2019
Accepted: November 20, 2019
Published: November 20, 2019

DOI: 10.1021/acsnano.9b07805
ACS Nano 2019, 13, 14348−14356

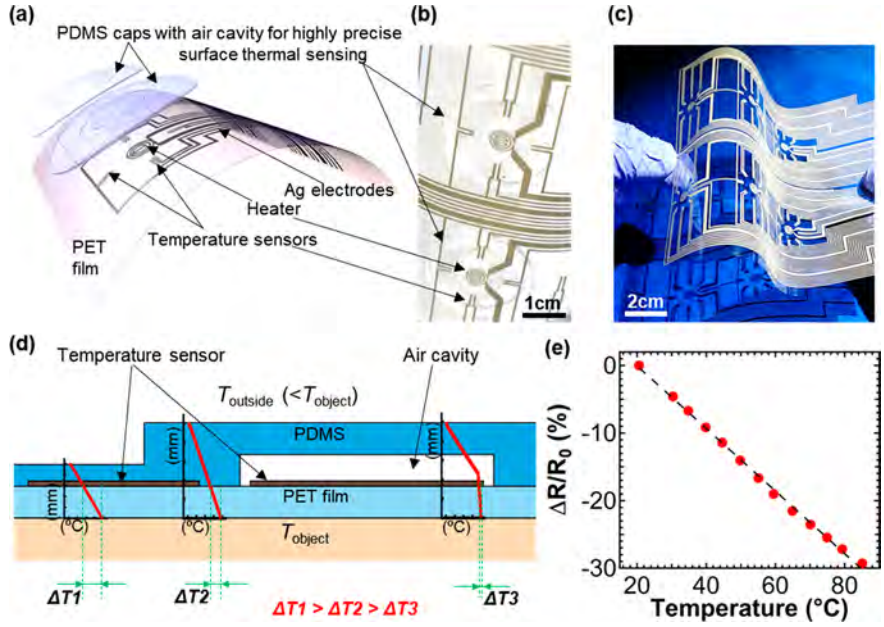

Figure 1. Thermal management-based flexible sensors. (a) Schematic of flexible flow sensors insulated by PDMS air cavities and (b) the corresponding photo. (c) Photo of a large-scale flexible thermal flow sensor array. (d) Principle of the temperature variation using different thermal shields (thickness and structure w/wo air cavity). Inset red graphs are thermal distributions along the material thickness extracted from FEM simulations when the top surface has a lower temperature ($T_{outside}$) than the bottom temperature (T_{object}). ΔT is the temperature difference between T_{object} and the temperature sensor surface (T_{sensor}) at $T_{outside}$. (e) Normalized resistance change ratio of the temperature sensor as a function of temperature.

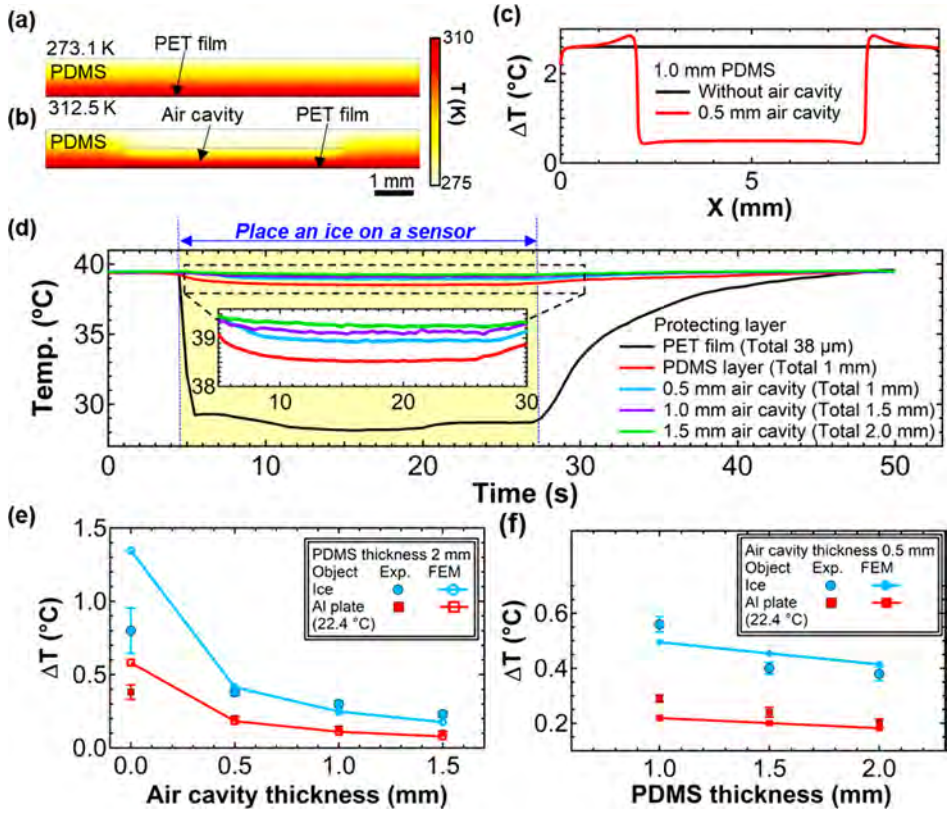

Figure 2. Fundamental characteristics of the temperature variation based on thermal management. FEM simulations of the heat distribution for devices (a) without and (b) with an air cavity. (c) Calculated temperature change between both sides of the PET film extracted from FEM simulations. (d) Real-time measurements of different thermal insulators on the sensor affected by ice on top of the sensor. Experimental and calculated ΔT ($T_{object} - T_{sensor}$) as functions of (e) air cavity and (f) PDMS thicknesses influenced by ice and the Al plate.

DOI: 10.1021/acsnano.9b07805
ACS Nano 2019, 13, 14348−14356

thermal-based or transduction flexible sensors for emerging Internet of Things (IoT) applications.

RESULTS AND DISCUSSION

To precisely monitor the targeted thermal intensity on unusual surfaces without being influenced by uncertain environments, air, which is a superior facilely accessible insulator with a low thermal conductivity (~0.024 W m^{-1} K^{-1} at 0 °C), is applied. Polydimethylsiloxane (PDMS) caps embedded with air cavities are seamlessly integrated onto flexible temperature sensors by a solution-based process. To demonstrate the reliability of the air cavity-protected temperature sensors, a large-scale flexible thermal flow sensor array is developed based on the calorimetric sensing mechanism (Figure 1a–c). This flexible thermal flow sensor can monitor the air flow characteristics on diverse surfaces due to its flexibility and accurate detection of heat transfer. Figure 1c shows a flexible thermal flow sensor array sheet where each pixel consists of eight temperature sensors surrounding a heater. Each sensor represents a different air flow orientation. The kernel concept of the air cavity-shielded temperature sensor is to dramatically decrease the temperature difference (ΔT) between the objective surface and the temperature sensor surface, allowing precise monitoring of the thermal status of the targeted surfaces (Figure 1d). The inset in Figure 1d shows the temperature profiles extracted by the finite element method (FEM). Although increasing the thickness of the PDMS insulators reduces ΔT ($\Delta T1$ to $\Delta T2$ in Figure 1d), ΔT is still too large to detect small temperature changes from the objective surface. In contrast, employing a PDMS film embedded with an air cavity drastically reduces ΔT ($\Delta T3$ in Figure 1d).

As a key thermal sensing element, a highly reliable flexible temperature sensor consisting of solution-based SnO_2 nanoparticles and single-walled carbon nanotubes is applied.[18,19] The sensors are integrated on a polyethylene terephthalate (PET) film with screen-printed silver (Ag) as the interconnect electrodes. Then the polymer is encapsulated for long-term stability. The resistance R of the temperature sensor decreases linearly as the temperature increases and exhibits a negative temperature coefficient behavior (Figure 1e). Owing to an electron-hopping mechanism, R can be expressed as a function of temperature as

$$R = R_0 \exp\left(\frac{E_a}{2kT}\right) \tag{1}$$

where R_0 is the resistance at the preliminary temperature, k is the Boltzmann constant, E_a is the activation energy, and T is the measured temperature. The trend in the resistance variation agrees well with this equation. A long-time testing of the flexible temperature sensor was performed using a commercial environmental oven by changing the temperature from 0 to 44 °C, presenting a highly stable output (Figure S1). The flexible temperature sensors have an average sensitivity of 0.97 ± 0.62%/°C extracted from 96 devices (Figure S2). The sensitivity is high enough for the application demonstrated in this study. Owing to the relatively high sensitivity variation from sample to sample, output temperature was calibrated by using each temperature sensor characteristic.

First, it is crucial to investigate the heat transfer behavior within different barriers. Parts a and b of Figure 2 show the FEM results of the two-dimensional spatial heat distribution in PDMS with and without air cavities on a PET film, assuming that the temperatures of the bottom and top edges are 312.5 and 273.1 K, respectively. Owing to the temperature difference between the two plane surfaces, energy is transferred from the warmer to the colder end via steady-state thermal conduction, which follows Fourier's law[20]

$$q = -k\Delta T \tag{2}$$

where q is the heat flux, k is the thermal conductivity, and ΔT is the temperature gradient. The heat transfer in PDMS with an air cavity is dramatically suppressed due to the low thermal conductivity of air, allowing the temperature to be precisely measured. More intuitively, ΔT between the surfaces of the temperature sensor and the object is extracted (Figure 2c). In the region where only PDMS is in contact with PET film, ΔT is approximately 2.6 °C. In contrast, ΔT significantly drops to 0.5 °C in the area in contact with the air cavity, indicating that the air cavity is a superior thermal insulator.

To explore the optimal structures as thermal barriers for temperature sensors, real-time measurements were conducted by placing ice on the temperature sensors covered by different thermal shields (Figure 2d). The temperature sensors were placed on a heat source (hot plate) at a constant temperature of 39.4 °C (Figure S3a). The temperature dramatically decreases by approximately 11.2 °C using a PET film as a protection layer due to the film thickness (38 μm) and relatively high thermal conductivity (~0.14 W m^{-1} K^{-1} at 23 °C). Assuming that the PDMS layer and PET film have similar thermal conductivities, the temperature change becomes smaller as the thickness of the protective PDMS layer increases. However, the temperature variation (nearly 1 °C) is too high to precisely monitor the temperature in practical sensing applications. To further reduce the temperature change, PDMS layers with air cavities and varying thicknesses were applied as thermal shields. The temperature drop tends to be quite small as both PDMS and the air cavity become thicker (Figure 2d, inset). Specifically, when the thicknesses of PDMS and the air cavity are 2.0 and 1.5 mm, respectively, the temperature becomes almost steady with a very subtle change of ~0.2 °C. This is a nearly 50-fold and 4-fold enhancement compared to the devices using a PET film and 2.0 mm thick PDMS as thermal barriers, respectively. Additionally, the relatively longer time measurements render a larger temperature drop for thermal insulators without air cavities (Figure S3b).

The temperature variations of the sensors with protective layers induced by an aluminum (Al) plate (temperature 22.4 °C) were monitored in real time (Figure S3c). Figure 2e plots ΔT as a function of air cavity thickness with a 2 mm-thick PDMS by extracting the temperature change before and after attaching a cold source. Both the experimental and theoretical results are shown. ΔT exhibits a similar descending tendency as the air cavity thickness increases because a PDMS cap with a thicker air cavity lowers the effective thermal conductivity. This yields a larger temperature gradient between the cold source and the temperature sensor, resulting in a smaller ΔT between the hot plate surface and the sensor for a given heat flux (Figure S3d). The experimental results agree well with the FEM simulations, except for PDMS without an air cavity as the protective layer, which is attributed to a contact issue between PDMS and the temperature sensor. At a constant air cavity thickness of 0.5 mm, the temperature variation gradually decreases with PDMS thickness (Figure 2f). Additionally, the thickness of PDMS without an air cavity increases up to 3.0 mm, and the temperature change due to the ice is relatively high (~0.55

DOI: 10.1021/acsnano.9b07805
ACS Nano 2019, 13, 14348–14356

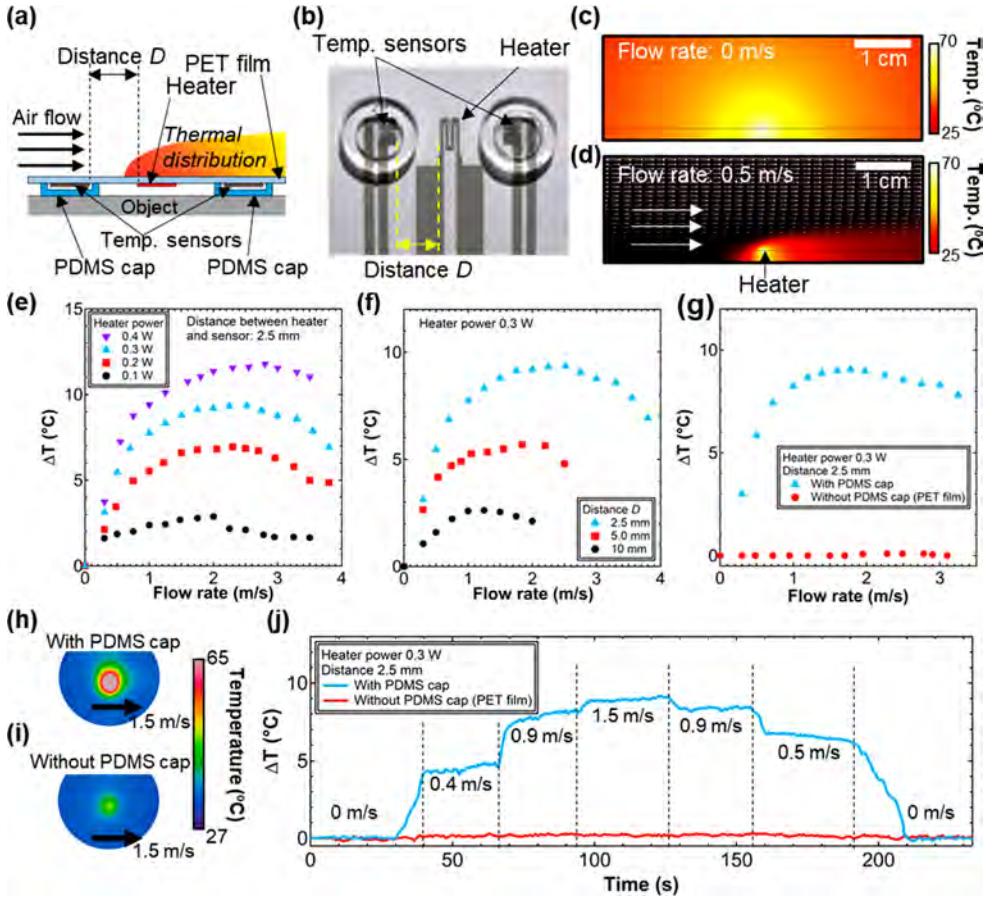

Figure 3. Fundamental properties of the flexible thermal flow sensors. (a) Schematic of a flexible thermal flow sensor on an object based on the principle of thermal regulation. (b) Photo of a flexible flow sensor with the downstream and upstream temperature sensors shielded by PDMS air cavities. FEM simulations of the thermal distribution (c) without and (d) with air flow. ΔT between the downstream and upstream of the thermal flow sensors measured by the integrated temperature sensors as a function of flow rate at different (e) heater powers and (f) distances between the temperature sensor and the heater. (g) ΔT of the thermal flow sensor with and without the PDMS air cavity on an Al plate. Infrared thermal images of the heater influenced by air flow with (h) a PDMS air cavity and (i) a PET film on the Al plate. (j) Real-time measurement of the thermal flow sensors on the Al plate.

°C) (Figure S3e). Likewise, by placing a heater (~73.6 °C) on the sensor, the absolute value of ΔT also presents a decreasing trend with air cavity thickness (Figure S4). To precisely detect the temperature while simultaneously preserving the flexibility of the temperature sensors, 1.5 mm thick PDMS with a 1.0 mm thick air cavity was employed for the following applications.

One promising use of the proposed flexible temperature sensors based on thermal management is to monitor the distribution of gas or water flow by manipulating thermal conduction and convection. These sensors have potential in many applications that demand monitoring of two-dimensional gas or fluid flow properties such as sweat, blood flow, respiration, spirometer, and capillary microcirculation. Although considerable advances have been made in thermal flow sensors that rely on bulk silicon-based microelectro-mechanical system (MEMS) technology, large-scale flow monitoring over diverse surfaces without disturbing the nature of pristine air flow remains a challenge. Herein we develop a flexible thermal flow sensor based on a calorimetric mechanism. It is composed of at least one heater and upstream and downstream temperature sensors seamlessly encapsulated by PDMS air cavities on PET films (Figure 3a,b). Flexible thermal flow sensors can monitor not only flow intensities but also flow directions over diverse surfaces such as highly thermal conductive objects. Furthermore, employing a screen-printing technique should form a macroscale flexible thermal flow sensor array, which can render a flow map on diverse surfaces, including a curved object. The optimized air cavities serve as thermal barriers to enhance the efficiency and accuracy of thermal convection induced by air flow. For an elementary calorimetric flow sensor, in principal, the temperatures of the upstream and downstream sensors in symmetrical positions with respect to the heater are identical at a flow rate of zero (Figure 3c). However, applying air flow generates an asymmetrical temperature profile, driving ΔT between the downstream and upstream transducers (Figure 3d), which is expressed as[21,22]

$$\Delta T = T_0(e^{\gamma_d l_d} - e^{-\gamma_u l_u}) \quad (3)$$

where T_0 is the temperature of the heater and l_d and l_u are the distances to the downstream and upstream sensors from the heater, respectively. Parameters γ_d and γ_u are associated with the velocity, thermal diffusivity of air flow, and boundary layer thickness.

An advantage of the proposed flow sensor is that it can detect relatively low flow velocities, which present an almost linear flow dependence with the sensitivity down to 0.08 °C·s/m (Figure 3e). At a certain air flow rate, ΔT reaches the peak position. Further increasing the air flow decreases ΔT because the

DOI: 10.1021/acsnano.9b07805
ACS Nano 2019, 13, 14348−14356

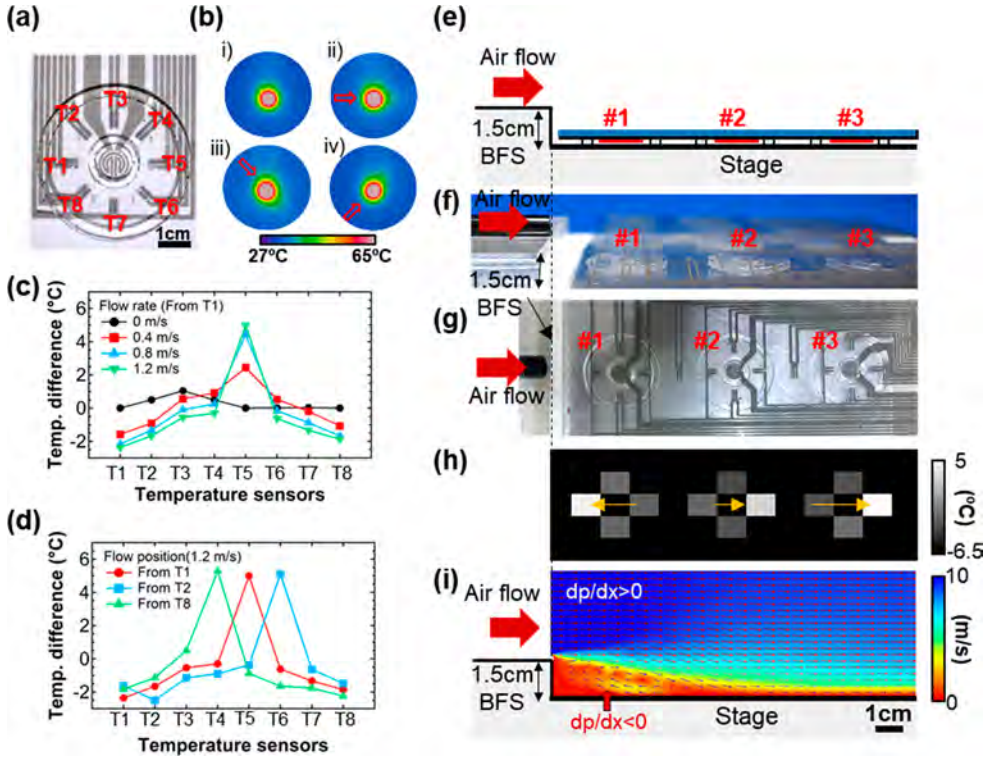

Figure 4. Flexible thermal flow sensors integrated with multiple temperature sensors. (a) Photo of the flow sensor comprised of eight temperature sensors surrounding a heater. (b) Infrared thermal images of the heater with (i) no air flow and (ii), (iii), (iv) air flow from different directions as indicated by the arrows. ΔT before and after air flow of each temperature sensor caused by different (c) flow rates and (d) flow positions. Applied heater power: 0.3 W. (e) Schematic of the setup to monitor flow distribution over a high thermal conductive plate with BFS. (f) Side-view and (g) top-view photos of (e). Each pixel consists of four temperature sensors and a heater. (h) Corresponding two-dimensional thermal change profile acquired from experimental mapping of the pixel signals. (i) Cross-sectional 2D FEM simulation of the air flow distribution over the BFS. Inset expression of *dp/dx* represents the air pressure gradient.

downstream sensor is cooled, which is consistent with the FEM results (Figure S5). Boosting the heater's power to 0.4 W saturates ΔT at a higher air flow rate of nearly 3.0 m/s. A similar behavior is observed for the flow sensor at a gap distance of 5 mm (Figure S6a). Notably, the temperature exhibits an almost positive linear variation as a function of the applied heater power (Figure S6b). Furthermore, the distance from the heater to the sensor determines the sensitivity and the maximum ΔT related to the air flow rate (Figure 3f). A smaller distance between the heater and temperature sensor leads to a higher sensitivity and a larger saturated ΔT with a higher air flow rate.

After investigating the fundamental characteristic of the flexible thermal flow sensor, the air flow over an aluminum (Al) plate was monitored (Figure 3g). Obviously, the flexible thermal flow sensor encapsulated by the PDMS air cavity works properly. Regardless of the air flow rate, the flexible flow sensor separated by a PET film layer over the Al plate surface shows ΔT of almost zero. Hence, the sensor cannot precisely measure the temperature change. This was verified by infrared thermal images of the heater. For the flow sensor protected by a PDMS air cavity, an anisotropic temperature distribution is generated due to the efficient convective thermal transfer along the orientation of air flow (Figure 3h). However, heat is still isotropically distributed even at an air flow rate of 1.5 m/s for the flow sensor without the PDMS cap (Figure 3i). Furthermore, the temperature of the heater dramatically decreases, owing to the conductive energy transfer from the heater to the Al plate provided with a high thermal conductivity (237 W m^{-1} K^{-1}). Thus, neither the upstream nor downstream sensor can precisely monitor the desired temperature, as discussed in the previous section. As a proof of concept for a practical application of the proposed flexible thermal flow sensor, the air flow was successfully detected over the Al plate surface in real time (Figure 3j). For the thermal flow sensor encapsulated by the PDMS air cavity cap, ΔT gradually increases as the air flow rate is increased from 0 to 1.5 m/s. In contrast, the thermal flow sensor without the PDMS cap fails to monitor flow rate dynamically.

As elaborated in the previous section, the proposed flexible thermal flow sensor can simultaneously monitor the air flow intensity and direction. To maximize the capacity of flow sensing in various directions, eight temperature sensors homogeneously surrounding a heater were conceived and fabricated (Figure 4a). Without an applied air flow, the heat distribution is almost isotropic (Figure 4b (i)). Upon applying a certain air flow, the anisotropic thermal transfer depends on the air flow directions (Figure 4b (ii–iv)). Such a flow induced convective thermal transport influences the heat distribution, resulting in temperature variations of the temperature sensors (i.e., T1– T8). The air flow direction can be deduced by comparing the temperature change of each sensor (Figure 4c). As ΔT is defined by the temperature variation with and without air flow, ΔT of unit T5 shows a larger temperature change compared to the other units when air flow is generated from the T1 side. Hence, increasing the air flow rate enhances ΔT, which agrees well with the results discussed in Figure 3. Similar trends are also observed when the air flow comes from T2 and T8 (Figure S7). For example, three different flow directions generate three different peaks, as shown by T4–T6 in Figure 4d. These peaks correspond to the air flow

DOI: 10.1021/acsnano.9b07805
ACS Nano 2019, 13, 14348–14356

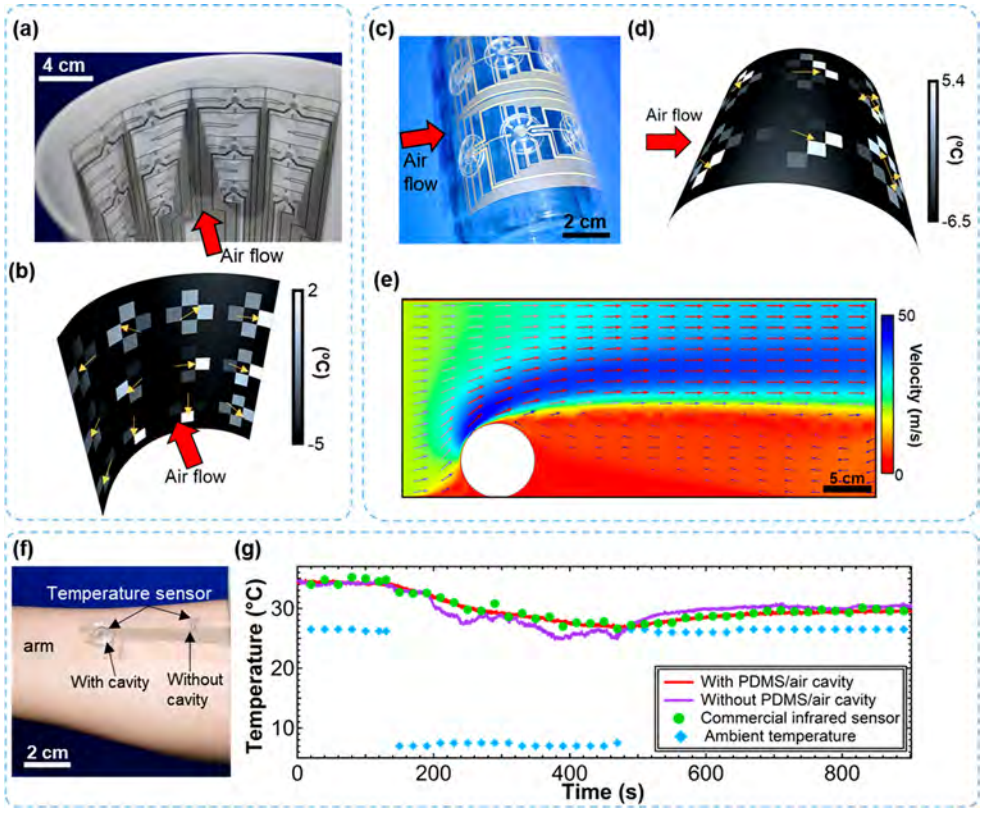

Figure 5. Demonstrations of macroscale flexible thermal flow sensor arrays and a wearable skin temperature sensor patch based on thermal management. (a) Photo of a macroscale flexible 4 × 3 thermal flow sensor array over a curved surface. (b) Thermal variation profile obtained from experimental flow mapping of the pixel signals. Arrows indicate the flow directions measured by the flexible flow sensors. (c) Photo of a flexible 3 × 2 thermal flow sensor array attached onto a pipe with a 7.5 cm diameter and (d) thermal mapping image under air flow corresponding to the flow direction monitoring. (e) 2D cross-sectional FEM simulation of the air flow distribution affected by a circular obstruction. (f) Photo of the skin temperature sensor patch with and without PDMS air cavity protection attached onto a volunteer's arm. (g) Real-time monitoring of skin temperature in different ambient environments. Measurement occurred at 10:39 pm on 23 February 2019 in Osaka/Japan.

directions from the upstream sensors. This suggests that a flexible flow sensor consisting of multiple temperature sensors has potential for large-scale flow monitoring. To demonstrate such a capability, three flow sensors arranged in a straight line were developed for flow separation and backflow monitoring over a high thermal conductive plate with a backward-facing step (BFS) (Figure 4e). The flow separation behavior usually occurs due to an adverse pressure-gradient-induced boundary layer separation or a geometrical obstacle. In many situations, separation is undesirable, including in aircrafts, wind turbine blades, micro aerial, and underwater vehicles because the airfoil efficiency decreases or large pressure fluctuations emerge.[23] Consequently, precise monitoring is crucial to reduce or even remove the flow separation effect. As a representative model for a flow separation dynamics study, BFS flow has attracted research and industry interests as it contributes to the investigation of the flow reattachment process by minimizing the flow separation process.[24] A controllable laminar flow serves as the inflow from a tube to the downstream step with the height of 1.5 cm (Figure 4f–g). A row of thermal flow sensors where each pixel is composed of four temperature sensors shielded by PDMS air cavities is placed on an Al plate. Figure 4h shows the measured two-dimensional (2D) thermal mapping extracted from real-time monitoring (Figure S8). The air flow direction over flow sensors #2 and #3 maintains the original flow orientation ($dp/dx > 0$). In contrast, the flow sensor closer to BFS indicates an inverse flow direction owing to the opposite pressure gradient ($dp/dx < 0$). Furthermore, the intensity of air flow over the middle flow sensor (#2) with a distance of approximately 6.0 cm to the step is slightly smaller than that of its downstream #3 pixel. This is attributed to the reattachment zone of the flow on the step. This flow separation was also observed in the FEM simulation (Figure 4i). Overall, the proposed flexible thermal flow sensors afford a pathway to investigate the phenomenon of separated flows that commonly occur in aerodynamic devices.

Since the flow sensors are fabricated on a flexible PET film, they can be attached onto a curved surface to detect air flow. As a proof of concept, a 4 × 3 large-scale thermal flow sensor array was fabricated and measured (Figure 5a and Figure S9). Due to the planar sheet-type thermal flow sensor array, it can monitor flow without disturbing the initial air flow characteristics. As shown in Figure 5b, injecting air flow from the central position of the flexible flow sensor array allows the air flow to spread along a curved surface. The flow distribution can be extracted according to the heat variation of each temperature sensor in the respective pixel (Figure 5b, arrows). To monitor the flow distribution over a complex surface precisely, a 3 × 2 flexible flow sensor array where each pixel consists of eight temperature sensors is demonstrated. The sensor array sheet was attached onto a tube with a 7.5 cm diameter and air inflow was from one side of the pipe (Figure 5c). Interestingly, the flow on the opposite side of

DOI: 10.1021/acsnano.9b07805
ACS Nano 2019, 13, 14348–14356

the pipe exhibits an unconventional distribution, as shown in the flow mapping image of Figure 5d extracted from the real-time flow monitoring (Figure S10). This is most likely attributed to the flow turbulence caused by the three-dimensional pipe structure working as the obstruction.[25] This turbulence flow was also simulated by the 2D FEM (Figure 5e).

This thermal management structure for a thin film-based flexible thermal sensor can be applied to a variety of applications. In addition to a thermal flow sensor array, this structure can be expanded to wearable sensing, which accurately monitors the skin temperature even if the ambient conditions change abruptly. To highlight the superior reliability of the proposed thermal-regulated temperature sensor, we experimentally compared the difference between the flexible temperature sensors with and without a PDMS air cavity by attaching a skin temperature sensor patch onto a volunteer's arm using a double-sided tape (Figure 5f). Initially, both temperature sensors provide almost the same result for the skin temperature (~34 °C) due to the thermal dynamic equilibrium (Figure 5g). After 140 s, the volunteer walked from a room at ~26.5 °C outside, which had a much lower ambient temperature of ~7.0 °C. This decreased skin temperature due to heat transfer between the human body and the environment. It can be seen that the intensity of the temperature sensor shielded by a PDMS air cavity exhibits a steady decreasing trend, and the values become 26.8 °C after several minutes. This result agrees well with that of a commercial infrared sensor. By comparison, the temperature sensor without a thermal-regulated structure shows a subtle discrepancy and is accompanied by slight temperature fluctuations. The value is more than 2 °C lower than that using a commercial sensor. This is because the outside ambient temperature and wind affect the output of a sensor without a thermal-regulated structure due to issues of heat transfer. When the volunteer reentered the room, the bare temperature sensor presents a faster increase in temperature compared to the two other sensors owing to the abrupt rise in the surrounding temperature. These results indicate that a flexible temperature sensor encapsulated by the thermal shield can precisely monitor the skin temperature without being influenced by external stimuli. Such accurate real-time monitoring of skin temperature changes coupled with other functional wearable sensors can provide clinically important physiological information such as fever, insomnia, cardiovascular diseases, metabolic functionality, and other syndromes.[26−29]

CONCLUSIONS

We demonstrate a versatile strategy to realize a highly accurate multifunctional flexible temperature-based sensing sheets based on efficient thermal management by introducing a low thermal conductive medium. By tailoring the parameters of thermal barriers, an approximately 50-fold enhancement is achieved with respect to the stability of thermal sensors, which are almost independent of external changes in the ambient conditions. The rational manipulation of heat convection and conduction can realize flexible thermal flow sensors to monitor air flow on a variety of surfaces. As a proof of concept, the flow distributions over the BFS and curved surfaces are successfully monitored by integrating a flexible thermal flow sensor array. Furthermore, a thermal-regulated flexible temperature sensor as a wearable sensor patch can precisely diagnose variations in the skin temperature in real time, even if the surrounding conditions change suddenly. Although skin-inspired thermal sensing has been around for almost two decades, traditional flexible temperature sensors usually focus on improving their characteristics such as sensitivity, response, intrinsic accuracy, repeatability, or portability.[30,31] Environmental conditions strongly affect the thermal detection due to the thin-film distance between the targeted surface and temperature sensor in flexible and thin film-based temperature sensors.[31,32] Our work, which is based on deliberate thermal management, not only realizes precise localized temperature sensing even if the external surroundings change suddenly but also implements thermal flow sensing over a large-scale spatial domain by elaborately manipulating heat transfer.

In the future, a plurality of tasks such as seeking lower thermal conductive media to form thinner effective thermal barriers, system integration with other sensors for exact healthcare monitoring, and a larger working range of thermal flow sensors need to be addressed. To further improve thermal sensing accuracy and enhance wearable comfort, vacuum-insulated panels are excellent candidates to serve as thermal insulations with thermal conductivity as low as 0.004 W/(m·K), providing around one-sixth the thermal conductivity of air. In addition, to minimize the electrical interconnections for macroscale applications, multiplexed detection strategy should be developed in future. Based on the concept and device demonstration, this platform should provide guidance to realize other thermal-based or transduction sensors that operate in harsh uncertain environment.

METHODS

Device fabrication. Ag electrodes were printed on a 38 μm thick PET film by a screen-printing method and were subsequently cured in an oven at 70 °C for more than 1 h. The active materials of the resistive temperature sensor were composed of mixtures of single-walled carbon nanotubes (concentration 0.01%, 20 μL), SnO_2 nanoparticles (40 mg), and deionized water (4 mL). A drop-casting method was then applied to form the solution over the Ag electrodes. The electrodes were cured at 110 °C for 10 min on a hot plate and washed with hot deionized water to remove residues. Afterward, the sensor was baked at 90 °C for 8 h. Finally, to protect the temperature sensor against scratching and humidity, a polymer (SIFEL2661, Shin-Etsu Chemical, Japan) was coated onto the sensor as the passivation layer. For flexible thermal flow sensors, the Ag electrode with a narrower line width was designed as the heater.

Thermal Shield Fabrication. PDMS air cavities were prepared from a mold fabricated by acrylic plates. A PDMS solution with a curing agent ratio of 10:1 (Dow Corning Sylgard 184) was poured into the mold. After curing at 70 °C for 2 h, PDMS was peeled from the mold. Subsequently, PDMS caps were attached onto the temperature sensors with the PDMS solution as the adhesion agent followed by baking at 70 °C for 2 h. The thicknesses of the PDMS caps (i.e., inner and outer depth) were precisely tuned by controlling the acrylic plate thickness. For thermal insulators without air cavities, the PDMS solution was directly poured onto the temperature sensor, which had dimensions defined by the acrylic plate mold, followed by oven curing. The acrylic plate mold was finally peeled from the device.

Characterization of Thermal-Regulated Temperature Sensors. The fundamental characteristics of the temperature sensor were investigated by a hot plate as the surface temperature rose in 5.0 °C steps. To study the thermal transfer behavior of the temperature sensors protected by different thermal barriers, the sensor was placed on a hot plate at a constant temperature of 39.4 °C. Then ice or an Al plate was applied on top of the thermal shields to induce a temperature gradient.

Demonstration. The air-flow rate was controlled by a commercial flow meter (Testo 425). The air flow was guided by an air tube with a 6.0 mm diameter. A DC power supply (Keysight Technologies, E36312A) afforded thermal energy for the heater, and the heater temperature was monitored by a commercial infrared thermal sensor (Keysight Technologies, U5855A). The flow was measured in real time

DOI: 10.1021/acsnano.9b07805
ACS Nano 2019, 13, 14348−14356

by connecting the sensor to a data logger (Hioki, LR8400) based on voltage divider circuits. For the real-time monitoring of skin temperature, the devices were attached onto the arm using a double-sided tape to make sure the seamless contact between the skin surface and sensors. The wearable temperature sensing was carried out in compliance with the protocol approved by Osaka Prefecture University.

FEM Simulations. Numerical simulations were performed based on FEM (COMSOL Multiphysics software). The thermal-barrier-dependent heat transfer behavior was based on the mode of heat transfer in solids. To study the flow sensing feature, physics models of laminar flow coupled with heat transfer in fluids and solids were applied. To investigate the flow distribution over BFS and around a circular obstacle, laminar flow was incorporated into the simulation. The adaptive mesh refinement approach was applied. All simulations were conducted in steady states.

ASSOCIATED CONTENT

Supporting Information

The Supporting Information is available free of charge at https://pubs.acs.org/doi/10.1021/acsnano.9b07805.

Long-time flexible temperature sensor test; sensitivity of 96 flexible temperature sensors; fundamental characteristics of the temperature variation based on thermal management; FEM simulations for flow sensors; fundamental property of thermal sensors; flexible thermal flow sensors integrated with multiple temperature sensors; real-time measurements of the thermal flow sensors over a high thermal conductive plate with BFS; real-time measurements of the thermal flow sensor array on a curved surface; real-time measurements of the thermal flow sensor array on a pipe (PDF)

AUTHOR INFORMATION

Corresponding Author

*E-mail: takei@pe.osakafu-u.ac.jp.

ORCID

Kaichen Xu: 0000-0003-4957-3144

Seiji Akita: 0000-0002-2116-4034

Kuniharu Takei: 0000-0001-9166-3747

Notes

The authors declare the following competing financial interest(s): The author is an inventor of two patent applications.

ACKNOWLEDGMENTS

This work was supported by JST PRESTO (JPMJPR17J5) and JSPS KAKENHI grants (JP17H04926 and JP18H05472). We thank Mr. Hiroki Ura, Dr. Hiroyuki Kato, and Mr. Takahiro Uchiyama at Japan Aerospace Exploration Agency (JAXA) for fruitful discussions.

REFERENCES

(1) McCluskey, F. P.; Podlesak, T.; Grzybowski, R. *High Temperature Electronics*; CRC Press: New York, 2018.

(2) Kwon, J. H.; Choi, S.; Jeon, Y.; Kim, H.; Chang, K. S.; Choi, K. C. Functional Design of Dielectric−Metal−Dielectric-Based Thin-Film Encapsulation with Heat Transfer and Flexibility for Flexible Displays. *ACS Appl. Mater. Interfaces* **2017**, *9*, 27062−27072.

(3) Madonna, V.; Giangrande, P.; Galea, M. Electrical Power Generation in Aircraft: Review, Challenges, and Opportunities. *IEEE Trans. Transport. Electrific.* **2018**, *4*, 646−659.

(4) Wang, X.-Q.; Tan, C. F.; Chan, K. H.; Xu, K.; Hong, M.; Kim, S.-W.; Ho, G. W. Nanophotonic-Engineered Photothermal Harnessing for Waste Heat Management and Pyroelectric Generation. *ACS Nano* **2017**, *11*, 10568−10574.

(5) Hsu, P.-C.; Song, A. Y.; Catrysse, P. B.; Liu, C.; Peng, Y.; Xie, J.; Fan, S.; Cui, Y. Radiative Human Body Cooling by Nanoporous Polyethylene Textile. *Science* **2016**, *353*, 1019−1023.

(6) Cai, L.; Song, A. Y.; Wu, P.; Hsu, P. C.; Peng, Y.; Chen, J.; Liu, C.; Catrysse, P. B.; Liu, Y.; Yang, A.; Zhou, C.; Zhou, C.; Fan, S.; Cui, Y. Warming up Human Body by Nanoporous Metallized Polyethylene Textile. *Nat. Commun.* **2017**, *8*, 496.

(7) Gao, T.; Yang, Z.; Chen, C.; Li, Y.; Fu, K.; Dai, J.; Hitz, E. M.; Xie, H.; Liu, B.; Song, J.; Yang, B.; Hu, L. Three-Dimensional Printed Thermal Regulation Textiles. *ACS Nano* **2017**, *11*, 11513−11520.

(8) Schleeh, J.; Mateos, J.; Iniguez-de-la-Torre, I.; Wadefalk, N.; Nilsson, P. A.; Grahn, J.; Minnich, A. J. Phonon Black-Body Radiation Limit for Heat Dissipation in Electronics. *Nat. Mater.* **2015**, *14*, 187−92.

(9) Loeblein, M.; Tsang, S. H.; Pawlik, M.; Phua, E. J.; Yong, H.; Zhang, X. W.; Gan, C. L.; Teo, E. H. High-Density 3D-Boron Nitride and 3D-Graphene for High-Performance Nano-Thermal Interface Material. *ACS Nano* **2017**, *11*, 2033−2044.

(10) Chen, J.; Huang, X.; Sun, B.; Jiang, P. Highly Thermally Conductive Yet Electrically Insulating Polymer/Boron Nitride Nanosheets Nanocomposite Films for Improved Thermal Management Capability. *ACS Nano* **2019**, *13*, 337−345.

(11) Gao, W.; Emaminejad, S.; Nyein, H. Y. Y.; Challa, S.; Chen, K.; Peck, A.; Fahad, H. M.; Ota, H.; Shiraki, H.; Kiriya, D.; Lien, D. H.; Brooks, G. A.; Davis, R. W.; Javey, A. Fully Integrated Wearable Sensor Arrays for Multiplexed *In Situ* Perspiration Analysis. *Nature* **2016**, *529*, 509−514.

(12) Zhao, S.; Zhu, R. Flexible Bimodal Sensor for Simultaneous and Independent Perceiving of Pressure and Temperature Stimuli. *Adv. Mater. Technol.* **2017**, *2*, 1700183.

(13) Zi, Y.; Lin, L.; Wang, J.; Wang, S.; Chen, J.; Fan, X.; Yang, P. K.; Yi, F.; Wang, Z. L. Triboelectric-Pyroelectric-Piezoelectric Hybrid Cell for High-Efficiency Energy-Harvesting and Self-Powered Sensing. *Adv. Mater.* **2015**, *27*, 2340−2347.

(14) Zou, Z.; Zhu, C.; Li, Y.; Lei, X.; Zhang, W.; Xiao, J. Rehealable, Fully Recyclable, and Malleable Electronic Skin Enabled by Dynamic Covalent Thermoset Nanocomposite. *Sci. Adv.* **2018**, *4*, No. eaaq0508.

(15) Xue, H.; Yang, Q.; Wang, D.; Luo, W.; Wang, W.; Lin, M.; Liang, D.; Luo, Q. A Wearable Pyroelectric Nanogenerator and Self-Powered Breathing Sensor. *Nano Energy* **2017**, *38*, 147−154.

(16) Krishnan, S. R.; Ray, T. R.; Ayer, A. B.; Ma, Y.; Gutruf, P.; Lee, K.; Lee, J. Y.; Wei, C.; Feng, X.; Ng, B.; Abecassis, Z. A.; Murthy, N.; Stankiewicz, I.; Freudman, J.; Stillman, J.; Kim, N.; Young, G.; Goudeseune, C.; Ciraldo, J.; Tate, M.; Huang, Y.; Potts, M.; Rogers, J. A. Epidermal Electronics for Noninvasive, Wireless, Quantitative Assessment of Ventricular Shunt Function in Patients with Hydrocephalus. *Sci. Transl. Med.* **2018**, *10*, No. eaat8437.

(17) Gao, W.; Nyein, H. Y. Y.; Shahpar, Z.; Fahad, H. M.; Chen, K.; Emaminejad, S.; Gao, Y.; Tai, L.-C.; Ota, H.; Wu, E.; Bullock, J.; Zeng, Y.; Lien, D.-H.; Javey, A. Wearable Microsensor Array for Multiplexed Heavy Metal Monitoring of Body Fluids. *ACS. Sens.* **2016**, *1*, 866−874.

(18) Yamaguchi, T.; Kashiwagi, T.; Arie, T.; Akita, S.; Takei, K. Human-Like Electronic Skin-Integrated Soft Robotic Hand. *Adv. Intell. Syst.* **2019**, *1*, 1900018−1900023.

(19) Nakata, S.; Shiomi, M.; Fujita, Y.; Arie, T.; Akita, S.; Takei, K. A Wearable pH Sensor with High Sensitivity Based on a Flexible Charge-Coupled Device. *Nat. Electron.* **2018**, *1*, 596−603.

(20) Lienhard, J. H. *A Heat Transfer Textbook*; Dover Publications, Inc.: Mineola, NY, 2011.

(21) Lammerink, T. S.; Tas, N. R.; Elwenspoek, M.; Fluitman, J. H. Micro-Liquid Flow Sensor. *Sens. Actuators, A* **1993**, *37*, 45−50.

(22) Nguyen, N.; Dötzel, W. Asymmetrical Locations of Heaters and Sensors Relative to Each Other Using Heater Arrays: A Novel Method for Designing Multi-Range Electrocaloric Mass-Flow Sensors. *Sens. Actuators, A* **1997**, *62*, 506−512.

(23) Chen, L.; Asai, K.; Nonomura, T.; Xi, G.; Liu, T. A Review of Backward-Facing Step (BFS) Flow Mechanisms, Heat Transfer and Control. *Therm. Sci. Eng. Prog.* **2018**, *6*, 194−216.

DOI: 10.1021/acsnano.9b07805
ACS Nano 2019, 13, 14348−14356

(24) Sujar-Garrido, P.; Benard, N.; Moreau, E.; Bonnet, J. P. Dielectric Barrier Discharge Plasma Actuator to Control Turbulent Flow Downstream of a Backward-Facing Step. *Exp. Fluids* **2015**, *56*, 70−85.
(25) Wood, J. N.; De Nayer, G.; Schmidt, S.; Breuer, M. Experimental Investigation and Large-Eddy Simulation of the Turbulent Flow Past a Smooth and Rigid Hemisphere. *Flow, Turbul. Combust.* **2016**, *97*, 79−119.
(26) Bariya, M.; Shahpar, Z.; Park, H.; Sun, J.; Jung, Y.; Gao, W.; Nyein, H. Y. Y.; Liaw, T. S.; Tai, L.-C.; Ngo, Q. P.; Chao, M.; Zhao, Y.; Hettick, M.; Cho, G.; Javey, A. Roll-to-Roll Gravure Printed Electrochemical Sensors for Wearable and Medical Devices. *ACS Nano* **2018**, *12*, 6978−6987.
(27) Xu, K.; Lu, Y.; Honda, S.; Arie, T.; Akita, S.; Takei, K. Highly Stable Kirigami-Structured Stretchable Strain Sensors for Perdurable Wearable Electronics. *J. Mater. Chem. C* **2019**, *7*, 9609−9617.
(28) Kim, J.; Sempionatto, J. R.; Imani, S.; Hartel, M. C.; Barfidokht, A.; Tang, G.; Campbell, A. S.; Mercier, P. P.; Wang, J. Simultaneous Monitoring of Sweat and Interstitial Fluid Using a Single Wearable Biosensor Platform. *Adv. Sci.* **2018**, *5*, 1800880.
(29) Son, D.; Bao, Z. Nanomaterials in Skin-Inspired Electronics: Toward Soft and Robust Skin-like Electronic Nanosystems. *ACS Nano* **2018**, *12*, 11731−11739.
(30) Zhao, J.; Zhang, Y.; Huang, Y.; Xie, J.; Zhao, X.; Li, C.; Qu, J.; Zhang, Q.; Sun, J.; He, B.; Li, Q.; Lu, C.; Xu, X.; Lu, W.; Li, L.; Yao, Y. 3D Printing Fiber Electrodes for an All-Fiber Integrated Electronic Device *via* Hybridization of an Asymmetric Supercapacitor and a Temperature Sensor. *Adv. Sci.* **2018**, *5*, 1801114.
(31) Xu, K.; Lu, Y.; Takei, K. Multifunctional Skin-Inspired Flexible Sensor Systems for Wearable Electronics. *Adv. Mater. Technol.* **2019**, *4*, 1800628.
(32) Ota, H.; Chao, M.; Gao, Y.; Wu, E.; Tai, L. C.; Chen, K.; Matsuoka, Y.; Iwai, K.; Fahad, H. M.; Gao, W.; Nyein, H. Y. Y.; Lin, L.; Javey, A. 3D Printed ″Earable″ Smart Devices for Real-Time Detection of Core Body Temperature. *ACS. Sens.* **2017**, *2*, 990−997.

DOI: 10.1021/acsnano.9b07805
ACS Nano 2019, 13, 14348−14356